A Flexible Wireless Pressure Sensor Based on UHF RFID Technology

Minghao Xu, Chenbin Zhao, Xueguan Liu, Xinjian Chen, *Senior Member, IEEE*, and Baoqing Nie

***Abstract*— Passive wireless flexible sensors are attractive in the areas of wearable electronics, healthcare services, and smart robotics due to the advantages of simplified electrical connection, no requirement for power source, and long lifetime. In this article, a wireless passive flexible pressure sensor based on ultrahigh-frequency (UHF) radio frequency identification (RFID) technology is proposed. The sensor consists of three layers, including a flexible RFID tag, an absorptive layer of ferrite film, and a compressive separation sponge in between. As an external load applies on the sensor, the sponge layer gets compressed, and the separation distance between the RFID tag and ferrite film reduces. As a result, the strength of the backscattering signal received by an RFID reader decreases due to the increment on the absorption effect from the ferrite film. Importantly, this is the first passive UHF pressure sensor adopting a tag-sponge-ferrite film structure, providing a compact solution to wireless pressure detection in the UHF band. Theoretical simulations have been conducted to analyze the influence of the thickness of the separation layer on the strength of the backscattering signal of the sensor, from which the optimal design of the passive pressure sensor has been defined. The sensor shows a high sensitivity of −9.49 dBm/kPa in the pressure range of 1.39–2.57 kPa, and environmental stabilities (within 0.91%) to temperature changes (25 °C–45 °C) and relative humidity (RH) variations (43%RH–82%RH). Importantly, the wireless transmission distance between the sensor and the reader is more than 70 cm, which is 16.67 times higher than a single *LC*-based wireless pressure sensor. This facilitates to broaden the potential usages of wireless passive pressure sensors in the fields of wearable electronics. To demonstrate the utility, the sensor has been integrated with a cuff and a cushion to wirelessly monitor bandage pressures and body movements.**

***Index Terms*— Finite element analysis, pressure sensor, ultrahigh-frequency (UHF) radio frequency identification (RFID), wireless passive sensor.**

Manuscript received 15 February 2024; revised 14 June 2024; accepted 29 June 2024. Date of publication 8 August 2024; date of current version 22 August 2024. This work was supported in part by the Natural Science Foundation of Jiangsu Province of China under Grant BK20211308, in part by the National Natural Science Foundation of China under Grant 61601317, and in part by the Natural Science Foundation of the Jiangsu Higher Education Institutions of China under Grant 20KJB510001. The Associate Editor coordinating the review process was Dr. Yuan Gao. *(Minghao Xu and Chenbin Zhao contributed equally to this work.) (Corresponding author: Baoqing Nie.)*

Minghao Xu, Chenbin Zhao, Xueguan Liu, and Baoqing Nie are with the School of Electronic Information, Soochow University, Suzhou 215006, China (e-mail: 1031881482@qq.com; 430946860@qq.com; txdzlxg@suda.edu.cn; qixinbq@suda.edu.cn).

Xinjian Chen is with the School of Electronic Information and the State Key Laboratory of Radiation Medicine and Protection, Soochow University, Suzhou 215006, China (e-mail: xjchen@suda.edu.cn).

This article has supplementary downloadable material available at https://doi.org/10.1109/TIM.2024.3440414, provided by the authors.

Digital Object Identifier 10.1109/TIM.2024.3440414

I. Introduction

FLEXIBLE passive wireless sensors have gained widespread attention due to their excellent mechanical flexibility, high sensitivity, and simple construction [1]. Wireless transmission technologies, which implement in flexible passive sensors, typically include inductor (L) and capacitor (C) resonating technology [2], [3], [4], near-field communication (NFC) [5], [6], [7], and ultrahigh-frequency (UHF) radio frequency identification (RFID) [8], [9]. Among those, the UHF passive RFID sensing technique acts in the frequency range of 860–960 MHz and operates in a longer communication distance (typically tens of meters) compared with its wireless counterpart sensing technologies [10]. In general, there are two types of implementations of UHF RFID sensors depending on whether an integrated circuit (IC) is included or not. In a chip-free UHF RFID sensing configuration, an electromagnetic wave sent by a reader impinges on to the chip-free tag, and the signal is most backscattered at the resonant frequency of the tag antenna [11]. It intrinsically holds the advantages of mechanical flexibility, low production cost, and long operation lifetime. A chip-based UHF RFID sensing system typically includes a sensor, an IC, and an antenna [12]. The sensor component can be standalone or integrated with the chip or the antenna. For example, Carvajal's group introduces a UHF passive RFID sensor with a temperature sensing modulus in the RFID chip [13]. The integration of the sensor and the chip provides a reliable configuration but increases the chip size and cost. Alternatively, the antenna itself can serve as a sensing component. Similar to the chip-free RFID sensor, it exploits the changes in antenna behavior (e.g., resistance, capacitance, or inductance) caused by the external parameters to be measured [14]. Differently, in the chip-based design, the backscattered power is usually modulated through impedance mismatch between the tag antenna and the chip. Those passive UHF RFID sensors have been vastly demonstrated in detections of various parameters, such as PH [15], humidity [16], gas [17], structure cracks [18], [19], and human motion [20].

Wireless RFID pressure sensors enable remote transmission of pressure signals to the digital world without the assistance of a battery or a power source. Those sensors have been extensively utilized in smart devices, such as soft robots [21], electronic skins [22], human–machine interactive systems [23], and healthcare services [24]. Most of the state-of-the-art RFID pressure sensors in the UHF band implement on the chip-free

configuration. For example, Bao et al. develop a passive chip-free sensor with a pressure-dependent capacitive component to detect blood flow. The signal is transmitted through near-field electromagnetic induction [25]. Another RFID pressure sensor implements a circular patch resonator (tag) on a compressive 3-D polymer structure to estimate the complex permittivity of the polymer [26]. Those chip-free pressure sensors usually need bulk equipment, such as a vector network analyzer (VNA) to determine the resonant frequencies of the RFID tags. Instead, chip-based RFID tags are compatible with commercial portable readers, which can process multichannel tag data in a compact solution. To the best of our knowledge, there is only one pressure sensor reported in previous study by using a chip-based UHF RFID tag [27]. However, in this work, the pressure signal is detected through a commercial resistive pressure sensor, which is externally connected to the tag IC. This construction increases the overall device dimension and the production cost and reduces its wearability and integrity.

In this report, we present a flexible passive pressure sensor based on the UHF RFID technology. The sensor is composed of three flexible layers: a top flexible reflective layer (i.e., ferrite film), a bottom RFID tag layer including a flexible antenna and an RFID chip, and a compressive layer (i.e., deformable sponge) in between. An external pressure deforms the compressive sponge layer, reducing the distance between the reflective layer and the RFID tag. Consequently, the reflective layer largely alters the impedance of the antenna. Therefore, the impedance mismatch between the antenna and the RFID chip leads to a decrease in the received signal strength indication (RSSI) from the reader end. Notably, our design is the first passive UHF pressure sensor that adopts a tag-sponge-ferrite film structure, distinguishing from the existing UHF RFID wireless pressure sensors that separate the sensor and microcontrollers for signal sensing, data communication and processing [28]. Our method simplifies the sensor structure by using the RFID tag to serve dual duties of pressure sensing and data communication, providing a compact solution for passive wireless pressure sensing in the UHF band. Benefitting from the flexible ferrite film with a high permeability and the soft compressive layer with a low mass density, the sensor exhibited a high sensitivity of −9.49 dBm/kPa within the pressure range of 1.39–2.57 kPa. In addition, under repeated mechanical loads and varied environmental conditions, the sensor shows stable responses (the fluctuations are within 0.91%). Taking the advantages of wireless pressure sensing with a long communication distance, our UHF-RFID-based flexible passive pressure sensor successfully achieves bandage pressure measurements and leg movement monitoring wirelessly, demonstrating its great prospect in the areas, such as wearable electronics and smart robotics.

II. Material and Methods

A. Device Fabrication Process

The flexible passive pressure sensor comprises three layers, including a ferrite film, a deformable flexible sponge layer, and an RFID tag. The fabrication process simply included laser micromachining and device assembly. Specifically, laser micromachining was employed to trim the geometrical shapes of the ferrite films (Nanjing Advanced Magnetic Material Company Ltd.), the flexible sponge layer (Yongxin Sponge Products Company Ltd.), and adhesive tape (467MP, 3M). Next, the ferrite film and the RFID tag were bonded to the sponge layer according to alignment markers by using adhesive tape, from which the assembly of the wireless pressure sensor was completed.

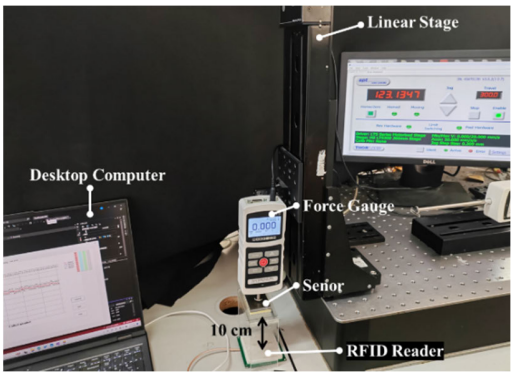

Fig. 1. Sensor performance characterization setup.

B. Device Sensitivity Characterization

To investigate the mechanical and electrical properties of the wireless pressure sensor, a customized calibration system was used, including a high-precision force gauge (M5-2, Mark-10 Corp) and a linear stage driven by a stepper motor (LTS300/M, Thorlabs Inc.). As shown in Fig. 1, a desktop computer controlled the movement of the linear stage and the force gauge and recorded the compression distance and the mechanical load on the sensor. A RFID reader (R200-C70, Shenzhen IOT Technology) was employed to receive the RSSI value from the sensor. The separation distance between the reader and the tag was fixed at 10 cm by an acrylic support. The pressure applied on the sensor was calculated from the ratio of the force to the sensor surface area. Two identical sensors were used and the RSSI values of each sensor were recorded two times under the pressures.

C. Environmental Factor Assessments

To investigate the impact of ambient temperature on the sensor performance, the sensor was heated by a hot plate with a constant relative humidity (RH) of 60%, and an infrared thermometer (i-Quip) was used to monitor the surface temperature on the sensor. For each temperature point, we recorded the sensor RSSI value ten times. Similarly, to assess the effect of RH, the sensor was placed in an airtight container at a constant room temperature of 25 °C, and a humidifier was employed to increase the humidity in the container. A commercial hygrometer was utilized to monitor the humidity level in the container and the sensor RSSI value was recorded ten times at each RH value.

III. Results and Discussion

A. Operating Principle

Fig. 2(a) and (b) illustrates the schematic and the photograph of the sensor, respectively. The equivalent circuit

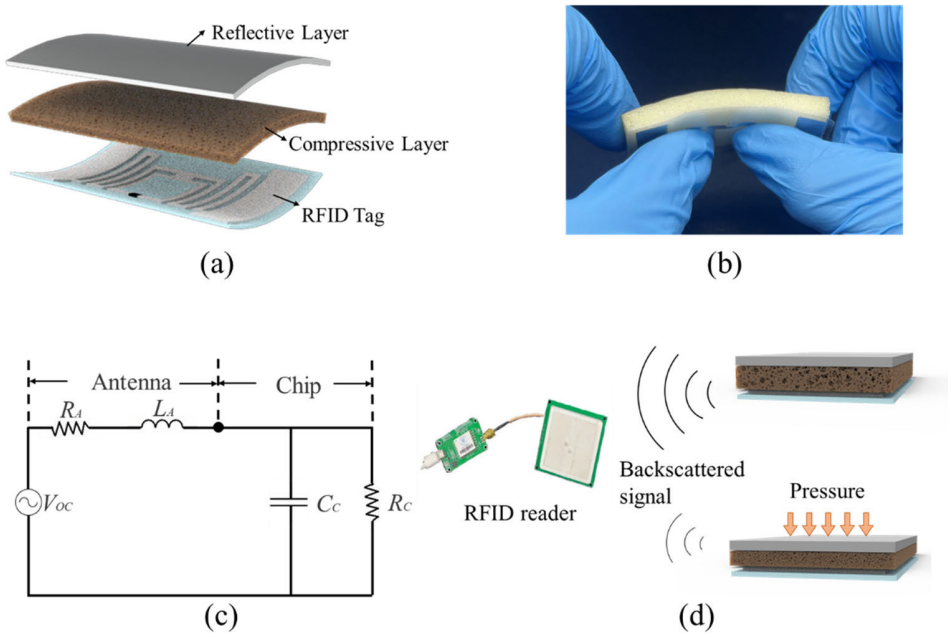

Fig. 2. (a) Schematic drawing of the structure of the pressure sensor. (b) Photograph of the flexible UHF passive RFID pressure sensor. (c) Equivalent circuit diagram of the sensor. (d) Illustration of the operation principle of the passive RFID sensor. The backscattering signal reduces its strength when the pressure is applied on the sensor.

diagram of the sensor is depicted in Fig. 2(c) [29]. It consists of a resistor (R_A) and an inductor (L_A) of the dipole-type antenna, and an input resistor (R_C) and a capacitor (C_C) of the RFID chip. V_{OC} represents the open-circuit voltage at the dipole antenna. The impedances of the antenna and the chip can be expressed as

$$Z_a = R_A + j\omega L_A \tag{1}$$

$$Z_c = R_C/(1 + j\omega C_C R_C). \tag{2}$$

In wireless transmission, an RFID reader first emits electromagnetic waves and transmits energy to the RFID tag. The antenna harvests the energy and activates the RFID chip. The RFID tag sends the backscattering signal to the RFID reader, during which the signal strength is tunable according to the impedance relationship between the chip and the antenna. Finally, the reader decodes the reflected signal to determine the RSSI. The value of RSSI can be expressed as

$$\text{RSSI} = G_r + K \tag{3}$$

where K represents the received signal strength from the reader excluding the gain of the sensor G_r when there is no pressure applied. K is related to the transmitting power of the reader, the gain of the reader antenna, and the path loss in the transmission of electromagnetic waves [30]. It can be estimated as a constant as long as the structure of the reader antenna and the separation distance of the reader and the sensor remain unchanged.

G_r in (3) refers to the gain of the sensor, which is associated with the maximum gain of the antenna $G_{\max}$ [31]

$$G_r = G_{\max} \times 4R_C R_A/|Z_c + Z_a|^2. \tag{4}$$

The maximum value of G_r is achieved when Z_c is conjugated to Z_a, indicating the optimal match between the antenna and the chip.

As illustrated in Fig. 2(d), when pressure is applied to the sensor, the sponge layer gets compressed, and the ferrite film with a high permeability and a low resistance to the magnetic flux approaches the bottom antenna, which largely changes the impedance of the antenna. As a result, the impedances of the antenna Z_a and the chip Z_c lose the optimal match, and subsequently, the gain of the sensor reduces, leading to a decrease in the RSSI.

B. Theoretical Analysis on the Tag Impedance, Reflection Coefficient, and Sensor Gain

To well design the structure of the sensor (e.g., the sponge layer and the ferrite film layer), we have performed a theoretical simulation on the gain, impedance, and return loss of the RFID antenna by using the finite element method (HFSS, Ansoft). Fig. 3(a) shows the sketch illustrating of the geometrical layout of the dipole antenna. Fig. 3(b) shows the gain pattern of the single-antenna structure, indicating that the antenna has the highest gain and radiation performance in the Z-axis direction (vertically above the antenna). The impedance spectrum of the antenna is shown in Fig. 3(c). The impedance at a center frequency of 915 MHz is found to be $(17.17 + 269.56i)\ \Omega$, which is conjugate with the chip (NXP UCODE7) impedance of $(17.6 - 274.8i)\ \Omega$, indicating a good matching between the antenna and the chip. In addition, the reflection coefficient (S11) is illustrated in Fig. 3(d). It reaches a value of -17.06 dB at 915 MHz.

To optimize the thickness of the sponge layer, we have investigated the influences of the initial separation distance between the ferrite film and the tag layer on the sensor gain G_r.

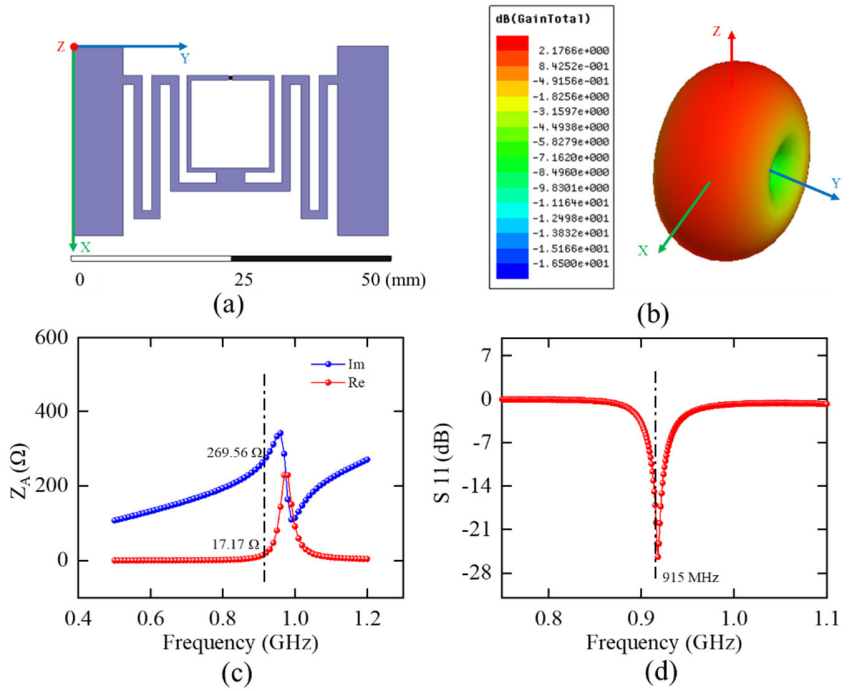

Fig. 3. Simulation investigations on the single RFID tag. (a) Layout of the antenna structure of the RFID tag. (b) Simulation results of the tag gain in a 3-D view. (c) Tag impedance spectrum. (d) Return loss spectrum. The dashed lines correspond to the frequency of 915 MHz.

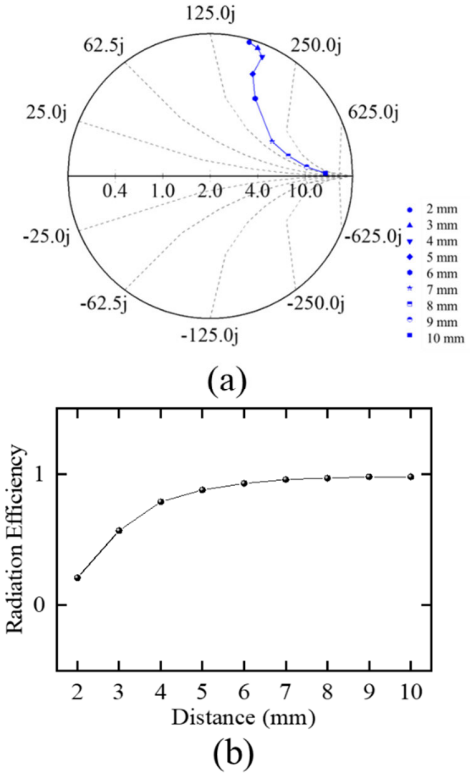

Fig. 4. Simulation investigation on the relationship between the ferrite film–tag separation distance and (a) antenna impedance in the Smith chart and (b) antenna radiation efficiency.

Fig. 4(a) shows the Smith circle diagram of the impedance of the antenna by varying the separation distance from 2 to 10 mm. As the reflective layer is away from the tag (e.g., 10 mm), the impedance of the antenna $(18.67 + 126.73i)$ is close to its original value. As the ferrite film moves close to the tag layer (e.g., 2 mm), the impedance of the antenna of $(0.06 + 166.48i)$ is increasingly different from the impedance of the chip. Therefore, the separation distance between the ferrite film and the RFID tag largely influences the antenna impedance, which in turn affects the matching degree of the antenna to the chip. In addition, Fig. 4(b) shows the relationship between the radiation efficiency of the antenna and the separation distance. The radiation efficiency increases as the ferrite film moves away from the antenna. It reaches 0.98 as the separation distance increases to 10 mm.

Fig. 5(a) presents the sensor gains G_r of the sensor in a 3-D view with the separation distances of 10 and 2 mm. Fig. 5(b) shows the relationship between the ferrite film–tag separation distance and G_r. It shows a similar trend with the curve in Fig. 4(b), indicating that the sensor gain G_r decreases as the tag–ferrite film distance reduces. The sponge layer with an initial thickness of 5 mm has been chosen in the following experiments considering that the sensor gain shows a large change (from 1.49 to −4.98 dB) as the thickness reduces from 5 to 2 mm.

C. Investigations on the Influences of the Compressive Layer on the Sensitivity

The pressure response of the sensor is highly influenced by the mechanical properties of the compressive layer. Here, we have utilized two sponge layers with different weight densities, serving as the compressive middle layer. Fig. 6(a) shows the photographs of the two sensors, in which the weight densities of the sponge layers are 35 kg/m^3 (35D, for sensor I) and 10 kg/m^3 (10D, for sensor II), respectively.

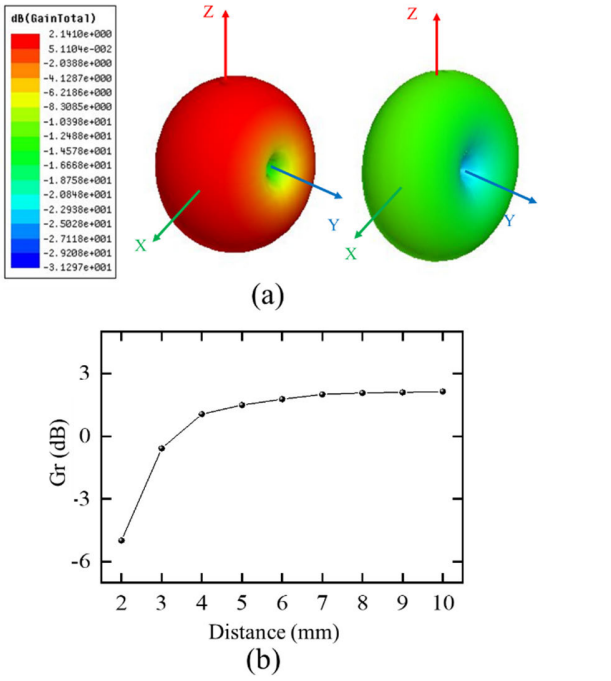

Fig. 5. Simulation results of (a) sensor gains in a 3-D view with the tag–ferrite film separation distances of 10 mm (left) and 2 mm (right). (b) Relationship of the sensor gains G_r and the separation distance.

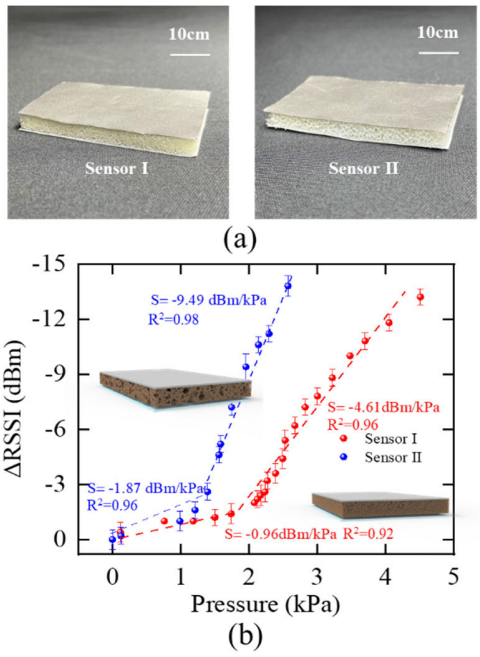

Fig. 6. (a) Photographs of the UHF passive RFID sensors with two different sponge mass densities. (b) Relationship between the RSSI of the two sensors and external pressures.

As the external reader couples to the sensors, they both have an initial RSSI value of −27 dBm, indicating the consistency of the sensors. Fig. 6(b) presents the sensitivities (defined as $S = \Delta\text{RSSI}/\text{Pressure}$) of the two types of sensors. As expected, when the applied pressure increases, the sensor gain decreases, and therefore, the RSSI decreases. Both sensors show a segmentation phenomenon in the whole pressure ranges.

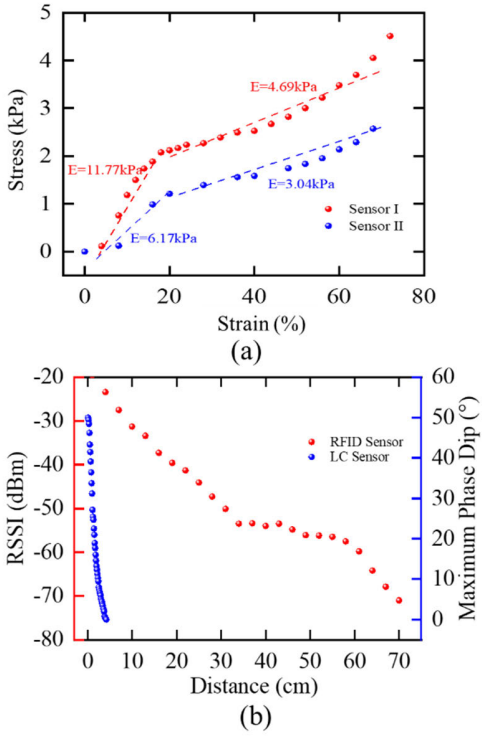

Fig. 7. (a) Stress–strain curves of the two types of the sensors. (b) Comparison on transmission distance between the RFID sensor and the *LC* sensor.

For sensor I, the sensitivity is −0.96 dBm/kPa in the pressure range of 0–2.07 kPa and increases to −4.61 dBm/kPa after the applied pressure exceeds 2.07 kPa. For sensor II, the sensitivity is −1.87 dBm/kPa in the pressure range of 0–1.39 kPa and increases to −9.49 dBm/kPa when the pressure exceeds 1.39 kPa.

The linearity of the sensor can be estimated through the sensitivity curve. A simple linear regression fitting is considered for the two sensors under different pressure windows. The two sensors exhibit good linearity in each pressure window with a coefficient of R^2 close to unity. In addition, the sponge density dominates the overall pressure range of the sensor. After the pressure exceeds 4.5 kPa (for sensor I) or 2.5 kPa (for sensor II), the RSSI signal decreases to a level that cannot be detected by the reader.

The phenomenon of segmented sensitivities is attributed to the mechanical properties of the sensors. Fig. 7(a) plots the stress–strain curves of the two sensors. Sensor I has a high Young's modulus ($E = 11.77$ kPa) in the low-pressure region (0–2.07 kPa) and a low Young's modulus ($E = 4.69$ kPa) in the high-pressure region (>2.07 kPa). For sensor II, Young's modulus drops from 6.17 to 3.04 kPa as the stress exceeds 1.39 kPa. This is a coincidence with segmented pressure regions in Fig. 6(b). Sensor I is used for the subsequent experiments considering its wider detection range.

Our pressure sensor utilizes UHF RFID technology for wireless and passive pressure transmission, which provides the advantage of longer transmission distance compared to other passive sensors, such as the *LC*-based pressure sensor. Here, we have compared the transmission distance of our UHF wireless RFID pressure sensor and a single typical *LC*-based

passive pressure sensor with a comparable size of 3 cm × 3 cm × 0.1 mm. The transmission distance of the *LC* resonant pressure sensor is determined through the phase dip method in the phase spectrum of an external reader [32]. In general, when the phase of the reader at the resonant frequency of the *LC* sensor drops to a minimum detectable level, the distance between the sensor and the reader is the maximum transmission distance. For the UHF RFID-based pressure sensor, a commercial reader (Impinj R2000-based modulus, Shenzhen IOT Technology) is used to receive the RSSI, and the maximum transmission distance is determined when the RSSI is lower enough (−71 dBm) that the reader cannot acquire the reflected signal from the sensor anymore. Fig. 7(b) illustrates the phase dips at the resonant frequencies of the *LC* sensor (blue dots) and the RSSI value of the UHF wireless RFID sensor (red dots) along with the distances between the sensor and the reader. The maximum transmission distances are 4.2 and 70 cm for the *LC* sensor and UHF-RFID sensor, respectively. A significant improvement (of 16.67 times) in the transmission distance is achieved by the UHF passive RFID pressure sensor.

D. Characterizations on Mechanical Repeatability and Resolution

To investigate the mechanical repeatability, the RSSI value of the sensor has been recorded when a cyclic load is applied. Fig. 8(a) shows the time-dependent RSSI changes under a dynamic load (from 2.29 to 2.71 kPa) with a period of 20 s for ten cycles. The periodic responses of the RSSI values indicate a good repeatability of our UHF passive RFID sensor.

Fig. 8(b) shows the sensor responses to the pressure changes of 1.81 kPa (left, from 0 to 1.81 kPa) and 0.25 kPa (right, from 2.43 to 2.68 kPa). The RSSI of the sensor changes by 2 dBm under the two pressures. The reason for different pressures inducing the same RSSI response is attributed to the segmented sensitivity in different pressure regions, as presented in Fig. 6(b). Our sensor can detect a pressure as low as 0.25 kPa in a high-pressure region.

E. Characterizations on Environmental Influences

We have investigated the potential impact of environmental parameters on the sensor, including the influence of disturbances such as temperature and humidity. Fig. 9(a) illustrates the RSSI changes along with the RH ranging from 40% to 80% under a constant temperature of 25 °C and a 10-cm distance between the reader and the sensor. At each RH level, ten RSSI readings were taken. The average RSSI value fluctuates at a low level (within 0.89%) throughout the entire RH range. In addition, Fig. 9(b) shows the relationship between the sensor RSSI value and the temperature as the RH level maintains a constant at room conditions. Ten RSSI values at each temperature point were measured. The average RSSI value shows a slight fluctuation of 0.91% in the entire temperature range of 25 °C–45 °C. The RSSI fluctuations induced by variations in RH levels and temperatures are corresponding to small pressure values (within 0.17 kPa), which can be negligible in the detections of human motion activities.

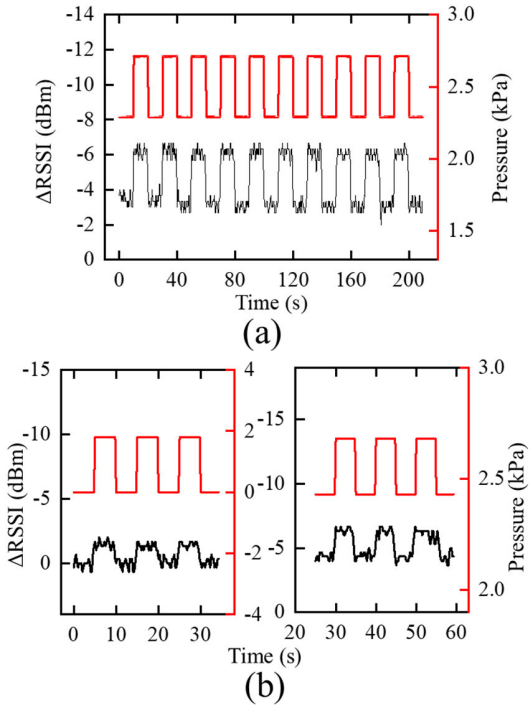

Fig. 8. (a) Sensor responses (black curve) under a repetitive mechanical load of 2.29–2.71 kPa (red curve). (b) Time-dependent RSSI changes under a low-pressure region (from 0 to 1.81 kPa) and a high-pressure region (from 2.43 to 2.68 kPa).

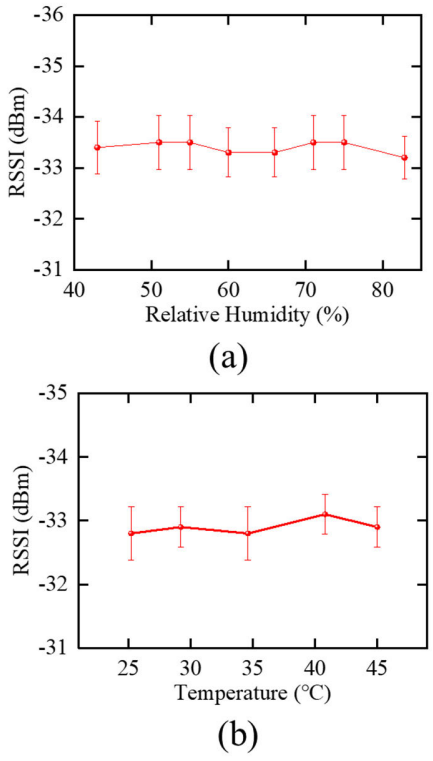

Fig. 9. Sensor responses to different (a) relative humidity levels and (b) environmental temperatures.

F. Investigation of the Impact of the Reader-Sensor Distance

As indicated in equation (3), the RSSI is related to the path loss in the transmission of electromagnetic waves and therefore sensitive to the reader–tag distance. Here, we have

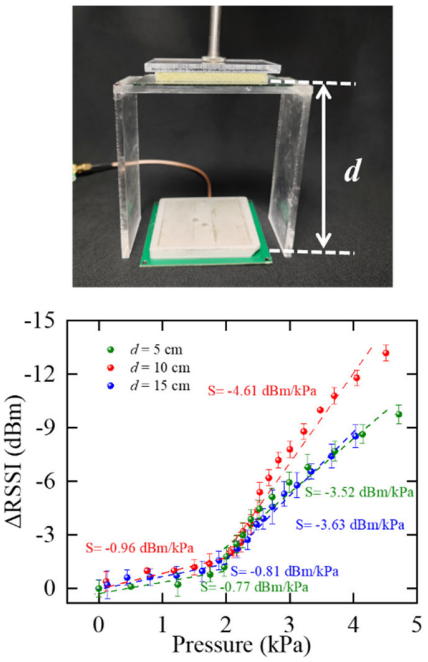

Fig. 10. Investigation on the impact of the reader–tag distance. Photograph of the experiment setup along with the comparison on the device sensitivities with three different reader–tag distances.

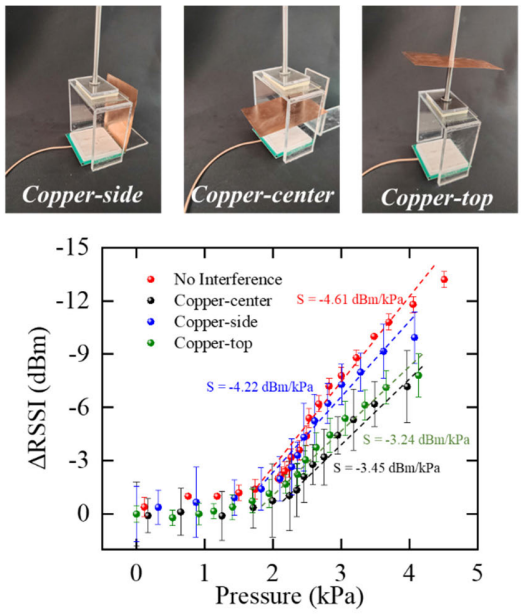

Fig. 11. Investigation on the impact of a surrounding copper plate. Photographs of the experiment setup with three locations of the copper plate. Comparison on the device sensitivities with the three different copper locations.

investigated the influence of the reader–tag distance on the device sensitivity. As shown in Fig. 10, the device shows a sensitivity of −4.61 dBm/kPa in the pressure region of 2–5 kPa under the reader–tag distance of 10 cm. The sensitivity decreases by around 22% at the distances of 5 and 15 cm. The impact of the distance variation can be reduced by using a dual-tag architecture [33].

G. Investigation of the Impact of Surrounding Objects

The device sensitivity has been compared when the surrounding substance changes. As shown in Fig. 11, a copper plate was placed on the side of the sensor–reader calibration system with a center distance of 2 cm (“copper-side” case), between the sensor and the reader with a distance of 5 cm to the sensor (“copper-center” case), or on the top of the sensor with a distance of 5 cm (“copper-top” case). In the copper-side case, the pressure sensitivity is almost consistent with the case of no copper (no interference) except for a slight reduction (by 8%) under the high-pressure level. In the copper-center and copper-top cases, the ΔRSSI obviously decreases by 29%. Besides, the error bar of each pressure point increases by more than twice with the presence of the copper plate, indicating tht the metal material causes signal fluctuations. Therefore, metal interference should be avoided in practical usage.

Fig. 12 shows the influences of different objects that press on the sensing tag. A plate with different dimensions (i.e., 54 mm × 74 mm, 44 mm × 64 mm, or 34 mm × 54 mm) or made by different materials [i.e., plank, glass, and polymethyl methacrylate (PMMA)] presses on the sensor. As shown, those factors all post a minimal influence on the device performance.

According to those investigations, the proposed sensor is mainly sensitive to two factors, i.e., the reader–tag distance and nearby conductive objects (e.g., metals). Therefore, such parameters need to be kept constant for real sensing applications. Otherwise, the sensor needs to be recalibrated in new environmental conditions.

H. Investigation of the Impact of Surrounding Background

The time-resolved RSSIs have been compared under different surrounding backgrounds. As shown in Fig. 13, the RSSI of the sensor is recorded under three scenes: laboratory, hallway, and outdoor. The RSSI is independent of the scenes, indicating that no multipath effect is observed. This is high because the RSSI is detected in a near-field condition (10 cm), and the multipath effect does not dominate the change of RSSI in this detection range.

I. Comparison on the State-of-the-Art UHF RFID Sensors

Table I compares the state-of-the-art UHF RFID sensors. As aforementioned, those passive UHF RFID sensors have been vastly utilized to detect various parameters, including pressure (see [25] and [26]), humidity (see [16] and [34]), structure cracks (see [19]), and human motion (see [33]), PH (see [15]). Specially for pressure detection, most of the devices adopt the antenna-based wireless transmission technique. In this case, bulk equipment, such as VNAs, is required to determine the resonant properties of the antenna/tag. In comparison, we utilize a sandwich sensing structure based on a chip-involved RFID tag. This design not only simplifies the sensor architecture but also is compatible to the portable reader for wireless data acquisition, realizing a compact pressure sensing solution at the UHF band.

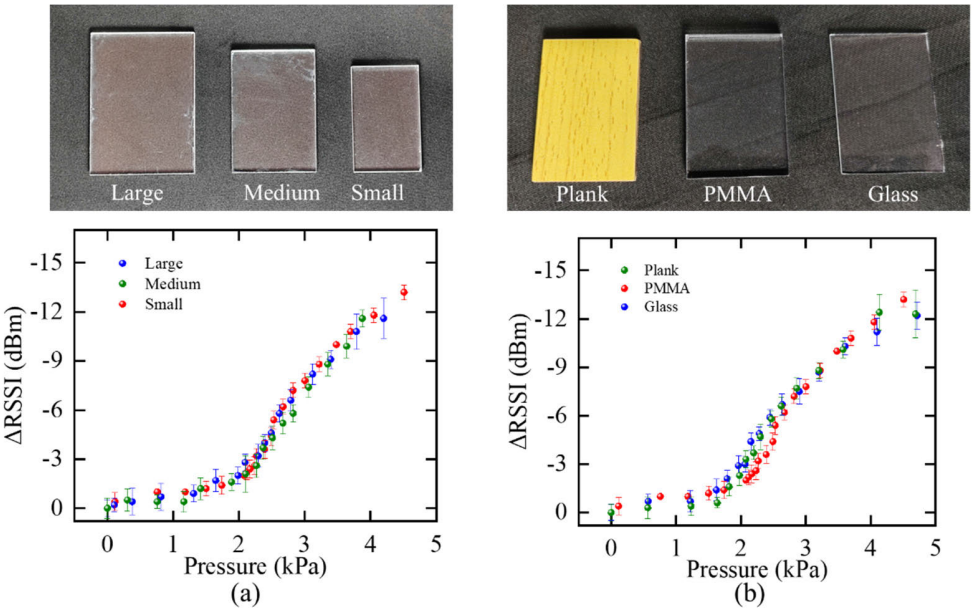

Fig. 12. Investigation on the impact of the object pressing on the sensor. (a) Comparison on the device sensitivity as three glass slides with different dimensions press on the sensor. (b) Comparison on the device sensitivities as three plates with different materials press on the sensor.

TABLE I
COMPARISON OF PASSIVE UHF RFID SENSORS

Wireless Sensing Technology	*Detection Parameter*	*Dimension (mm^2)*	*Measurement Setup*	*Reading Rang*	*Sensing Application*	*Ref.*
Chip-based RFID	Backscattered power	89 × 58	Reader-based	60 cm	Haptic	[33]
Chip-free UWB[1] RFID	Radar cross section	35 × 15	VNA-based	30 cm	Metal Crack	[19]
Chip-based RFID	RSSI	75 ×38	Reader-based	50 cm	Wetness	[16]
Chip-free UWB RFID	S parameter	-	VHA-based	-	PH	[15]
Chip-free RFID	S parameter	15.1 ×15.1	VHA-based	-	Humidity	[34]
Chip-free RFID	S parameter	30 × 30	VHA-based	5 mm	Pressure	[26]
Chip-free RFID	S parameter	5 × 20	VHA-based	<1 cm	Pressure	[25]
Chip-based RFID	RSSI	54 × 34	Reader-based	⩾10 cm	Pressure	This work

[1]*UWB: ultra-wideband*

J. UHF Passive RFID Sensor for Wireless Bandage Pressure Measurements

Measuring bandage pressures under various movements and postures can assist in evaluating the efficacy of bandages during physical activity [35], [36], [37]. Traditional measurement methods require the use of wired sensors, which may restrict the flexible motion of patients. Here, we have developed a smart compression cuff by integrating our flexible UHF passive RFID sensor to wirelessly measure the interactive pressures [see Fig. 14(a)]. The smart cuff is wrapped on a volunteer's arm, and the reader is placed beside the arm with a distance of 10 cm. The wrapping tension is regulated by inflating and deflating to the cuff through an air intake. Three different tensions, i.e., loose (red line), medium (blue line), and tight (green line) in Fig. 14(b), have been sensitively quantified by our sensor with the output pressures of 1.2, 2.4, and 3.2 kPa. It also successfully detects the pressure changes as the volunteer bends his arm at three angles of 0°, 45°, and 90°. Particularly, in the low wrapping tension, arm bending at different angles has little effect on compression pressures (the increment is only 0.03 kPa), while for the medium and high wrapping tension, the arm bending activity results in significant pressure increments of 0.94 and 1.11 kPa, respectively.

We have further measured the compression pressures as the volunteer stands up straight or squats with the cuff wrapping on his lower leg [see Fig. 14(c)]. The cuff is wrapped with the tension of loose, medium, or tight. The pressure recorded by our sensor is shown in Fig. 14(d) as the volunteer repeats the actions of standing straight and squatting five times. The posture of squatting leads to an increase in cuff pressure in comparison to that for the standing upright posture. This is

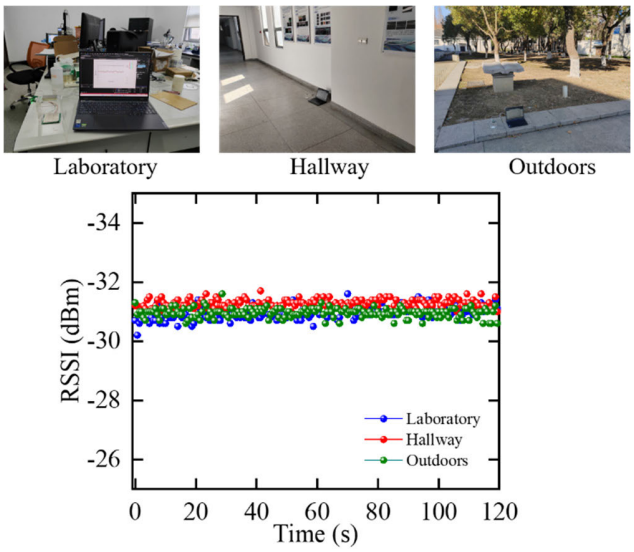

Fig. 13. Investigation of the impacts of surrounding backgrounds on the RSSIs.

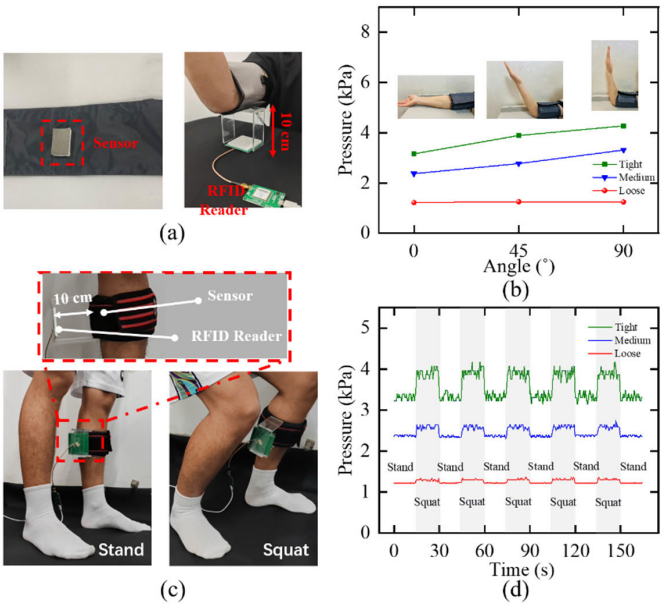

Fig. 14. (a) Photograph of the smart cuff, in which the sensor is attached inside the cuff. (b) Smart cuff can distinguish arm bending angles with different wrapping tensions. (c) Pictures illustrate that the volunteer wears the cuff on his leg and stands upright (left) or half squats (right). (d) Time-dependent sensor outputs as the volunteer repeats the postures of standing upright and half squatting with different wrapping tensions.

possible because the muscles in the lower leg are more active and engaged when squatting, which results in a higher level of compression pressure from the cuff. In addition, a smart cushion has been developed based on our UHF passive RFID pressure sensor for wireless sitting pressure measurements (Fig. S1, see the Supplementary Material).

K. UHF Passive RFID Sensor for Wireless Leg Movement Monitoring

Body movements convey much individual information, such as behavioral characteristics and physiological functions. Here, the smart cuff has been utilized to monitor the movement of a leg when a person is walking. Considering that the RSSI of the sensor is dependent on the tag–reader distance during walk, a dual-tag topology has been applied to reduce the distance influences on the output signal.

As shown in Fig. 15(a), the dual-tag-based pressure sensor includes two components: a sensing part/tag, which is the same as the previous sensor, and a reference part/tag, which excludes the ferrite film and the sponge layer from the sensor. The dual-tag sensor with a dimension of 88 mm × 54 mm is attached to a cuff. After the cuff is wrapped on the volunteer's leg, the RSSIs of the two tags are recorded by the reader simultaneously when the volunteer walks slowly forward in front of the reader [see Fig. 15(b)]. Both tags change their RSSIs periodically at the same rate with the stride [see Fig. 15(c) and Video S1]. For the reference tag, the RSSI (blue dot line) varies due to the tag–reader distance changes in each step. For example, in the period during which the volunteer moves close to the reader (marked in the green region), the tag–reader distance decreases when the volunteer lifts his leg, which results in an intensive RSSI signal. On the contrary, the RSSI signal decreases when the volunteer puts down his leg. During the period of moving away from the reader (marked in the yellow region), the tag–reader distance rises when the volunteer lifts his leg, and accordingly, the RSSI reduces. For the sensing tag, its RSSI variation is contributed by two factors, i.e., the reader–tag distance and the cuff wrapping tension. Interestingly, in the first two-step cycles, the RSSI of the sensing tag shows very small fluctuations. This is because, as the volunteer lifts the leg, the reduced tag–reader distance leads to a growing RSSI; meanwhile, the increased wrapping tension contributes to a decreased RSSI. The two effects have been canceled. This distance impact can be generally removed by using the RSSI difference of the two tags ($RSSI_1$–$RSSI_2$). Fig. 15(d) shows time-solved $RSSI_1$–$RSSI_2$ during the walk. The amplitude of the signal remains around 19 dBm, indicating that the distance influence is greatly reduced in this dual-tag architecture.

Fig. 15(e) illustrates the $RSSI_1$–$RSSI_2$ variations when the volunteer walks in different scenes, i.e., a laboratory with the center tag–reader distance of 10 cm and a hallway with the center tag–reader distance of 10 or 30 cm. The differential RSSI variation is almost independent of the scenes. Fig. 15(f) illustrates that a person passes by the volunteer when he is walking. Fig. 15(g) shows the $RSSI_1$–$RSSI_2$ variations when the volunteer walks forward in the same stride as before, during which another volunteer gets close and then leaves away. There is no obvious interference on the RSSI output.

Although the cuff pressure cannot be obtained since there is no mechanical-to-electrical calibration for the dual-tag sensor, the results still can deliver information such as step paces. Importantly, this method can improve the robustness of the sensor to the distance interference. Future work could focus on the optimizations on the device designs and structural materials of this dual-tag pressure sensing method.

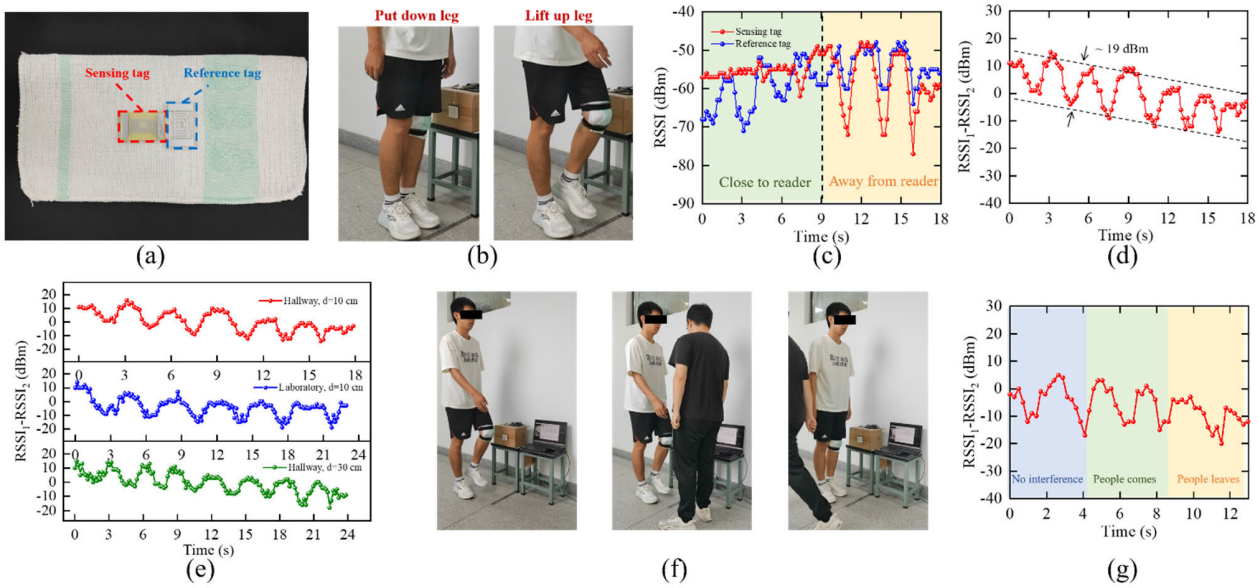

Fig. 15. (a) Photograph of a dual-tag sensor attaching on a cuff. The overall dimension of the dual tags is 88 mm × 54 mm. (b) Volunteer wears the cuff and slowly walks forward. The dual-tag sensor in the cuff faces the reader. (c) Time-resolved RSSIs of the two tags during walk. (d) Variation of the differential RSSI of the two tags ($RSSI_1$–$RSSI_2$) during walk. (e) Time-resolved $RSSI_1$–$RSSI_2$ curves when the volunteer walks in different scenes: a laboratory with the center tag–reader distance of 10 cm and a hallway with the center tag–reader distance of 10 or 30 cm. (f) Photographs showing people passing by the volunteer when he is walking. (g) Recorded $RSSI_1$–RSSI2 values in the scene shown in (f).

IV. Conclusion

In this article, a wireless passive pressure sensor utilizing UHF RFID technology is introduced for bandage pressure measurement and leg movement monitoring. This fully passive and wireless pressure sensor offers several key advantages.

1) By introducing an absorptive layer of ferrite film with high permeability, the sensor can largely change the gain of the antenna in the RFID tag and achieve a high device sensitivity of −9.49 dBm/kPa.
2) The RFID sensor is constructed in a compact architecture. It measures pressure signals in a wireless fashion with an improved communication distance compared to its counterparts based on the electromagnetic coupling technique. The UHF-RFID-based wireless pressure sensor with simple construction and mechanical flexibility shows promising usages in comprehensive wireless pressure distribution measurements in emerging fields, such as wearable electronics and smart robotics.

References

[1] A. Subrahmannian and S. K. Behera, "Chipless RFID sensors for IoT-based healthcare applications: A review of state of the art," *IEEE Trans. Instrum. Meas.*, vol. 71, 2022, Art. no. 8003920.

[2] Z. Dong, Z. Li, F. Yang, C.-W. Qiu, and J. S. Ho, "Sensitive readout of implantable microsensors using a wireless system locked to an exceptional point," *Nature Electron.*, vol. 2, no. 8, pp. 335–342, Aug. 2019.

[3] A. M. Beierle et al., "Rapid characterization of solid tumors using resonant sensors," *ACS Omega*, vol. 7, no. 36, pp. 32690–32700, Sep. 2022.

[4] M. Simic, A. K. Stavrakis, M. Radovanovic, A. Iqbal, V. Jeoti, and G. M. Stojanovic, "A portable device for passive LC sensors readout with low-coupling enhanced sensitivity," *IEEE Trans. Instrum. Meas.*, vol. 72, 2023, Art. no. 2001012.

[5] G. Zhang, P. Li, X. Wang, Y. Xia, and J. Yang, "Flexible battery-free wireless sensor array based on functional gradient-structured wood for pressure and temperature monitoring," *Adv. Funct. Mater.*, vol. 33, no. 2, Jan. 2023, Art. no. 2208900.

[6] A. Lazaro, R. Villarino, and D. Girbau, "A survey of NFC sensors based on energy harvesting for IoT applications," *Sensors*, vol. 18, no. 11, p. 3746, Nov. 2018.

[7] S. Han et al., "Battery-free, wireless sensors for full-body pressure and temperature mapping," *Sci. Translational Med.*, vol. 10, no. 435, p. 4950, Apr. 2018.

[8] N. Khalid, R. Mirzavand, and A. K. Iyer, "A survey on battery-less RFID-based wireless sensors," *Micromachines*, vol. 12, no. 7, p. 819, Jul. 2021.

[9] I. Ullah, R. Horne, B. Sanz-Izquierdo, and J. C. Batchelor, "RFID AC current sensing technique," *IEEE Sensors J.*, vol. 20, no. 4, pp. 2197–2204, Feb. 2020.

[10] A. Motroni, A. Buffi, P. Nepa, and B. Tellini, "Sensor-fusion and tracking method for indoor vehicles with low-density UHF-RFID tags," *IEEE Trans. Instrum. Meas.*, vol. 70, 2021, Art. no. 8001314.

[11] P. Sethy and S. K. Behera, "Chipless RFID sensors for bioimplants: A comprehensive review," *IEEE Microw. Mag.*, vol. 24, no. 7, pp. 41–60, Jul. 2023.

[12] F. Costa, S. Genovesi, M. Borgese, A. Michel, F. A. Dicandia, and G. Manara, "A review of RFID sensors, the new frontier of Internet of Things," *Sensors*, vol. 21, no. 9, p. 3138, Apr. 2021.

[13] J. Fernández-Salmerón, A. Rivadeneyra, F. Martínez-Martí, L. Capitán-Vallvey, A. Palma, and M. Carvajal, "Passive UHF RFID tag with multiple sensing capabilities," *Sensors*, vol. 15, no. 10, pp. 26769–26782, Oct. 2015.

[14] J. Zhang, G. Tian, A. Marindra, A. Sunny, and A. Zhao, "A review of passive RFID tag antenna-based sensors and systems for structural health monitoring applications," *Sensors*, vol. 17, no. 2, p. 265, Jan. 2017.

[15] T. Athauda, P. C. Banerjee, and N. C. Karmakar, "Microwave characterization of chitosan hydrogel and its use as a wireless pH sensor in smart packaging applications," *IEEE Sensors J.*, vol. 20, no. 16, pp. 8990–8996, Aug. 2020.

[16] M. Tekcin, M. Palandoken, and S. Kursun, "Wearable UHF-RFID sensor for wetness detection," *IEEE Access*, vol. 11, pp. 115179–115189, 2023.

[17] D. P. Mishra and S. K. Behera, "Resonator based chipless RFID: A frequency domain comprehensive review," *IEEE Trans. Instrum. Meas.*, vol. 72, pp. 1–16, 2023.

[18] S. Caizzone and E. DiGiampaolo, "Wireless passive RFID crack width sensor for structural health monitoring," *IEEE Sensors J.*, vol. 15, no. 12, pp. 6767–6774, Dec. 2015.

[19] A. M. J. Marindra and G. Y. Tian, "Chipless RFID sensor tag for metal crack detection and characterization," *IEEE Trans. Microw. Theory Techn.*, vol. 66, no. 5, pp. 2452–2462, May 2018.
[20] S. Amendola, L. Bianchi, and G. Marrocco, "Combined passive radiofrequency identification and machine learning technique to recognize human motion," in *Proc. 44th Eur. Microw. Conf.*, Oct. 2014, pp. 1044–1047.
[21] Y. Liu, B. Chen, W. Li, L. Zu, W. Tang, and Z. L. Wang, "Bioinspired triboelectric soft robot driven by mechanical energy," *Adv. Funct. Mater.*, vol. 31, no. 38, Sep. 2021, Art. no. 2104770.
[22] S. Lee et al., "A high-fidelity skin-attachable acoustic sensor for realizing auditory electronic skin," *Adv. Mater.*, vol. 34, no. 21, May 2022, Art. no. 2109545.
[23] Y. Zhang, M. Shafiei, J. Z. Wen, Z. Abbasi, and C. L. Ren, "Simultaneous detection of pressure and bending using a microwave sensor with tag and reader structure," *IEEE Trans. Instrum. Meas.*, vol. 72, 2023, Art. no. 9511311.
[24] W.-J. Deng, L.-F. Wang, L. Dong, and Q.-A. Huang, "LC wireless sensitive pressure sensors with microstructured PDMS dielectric layers for wound monitoring," *IEEE Sensors J.*, vol. 18, no. 12, pp. 4886–4892, Jun. 2018.
[25] C. M. Boutry et al., "Biodegradable and flexible arterial-pulse sensor for the wireless monitoring of blood flow," *Nature Biomed. Eng.*, vol. 3, no. 1, pp. 47–57, Jan. 2019.
[26] K. Brinker and R. Zoughi, "Tunable chipless RFID pressure sensor utilizing additive manufacturing," in *Proc. IEEE Int. Instrum. Meas. Technol. Conf. (I2MTC)*, May 2022, pp. 1–6.
[27] A. Rennane et al., "Design of passive UHF RFID sensor on flexible foil for sports balls pressure monitoring," *IET Microw., Antennas Propag.*, vol. 12, no. 14, pp. 2154–2160, Nov. 2018.
[28] X. Lin and B.-C. Seet, "Battery-free smart sock for abnormal relative plantar pressure monitoring," *IEEE Trans. Biomed. Circuits Syst.*, vol. 11, no. 2, pp. 464–473, Apr. 2017.
[29] G. Chakaravarthi, K. P. Logakannan, J. Philip, J. Rengaswamy, V. Ramachandran, and K. Arunachalam, "Reusable passive wireless RFID sensor for strain measurement on metals," *IEEE Sensors J.*, vol. 18, no. 12, pp. 5143–5150, Jun. 2018.
[30] K. Chang, *RF and Microwave Wireless Systems (Wiley Series in Microwave and Optical Engineering)*. New York, NY, USA: Wiley, 2000, p. 339.
[31] X. Wang, J. Zhang, Z. Yu, S. Mao, S. C. G. Periaswamy, and J. Patton, "On remote temperature sensing using commercial UHF RFID tags," *IEEE Internet Things J.*, vol. 6, no. 6, pp. 10715–10727, Dec. 2019.
[32] B. Nie et al., "Textile-based wireless pressure sensor array for human-interactive sensingg," *Adv. Funct. Mater.*, vol. 29, no. 22, May 2019, Art. no. 1808786.
[33] S. Kim, Y. Kawahara, A. Georgiadis, A. Collado, and M. M. Tentzeris, "Low-cost inkjet-printed fully passive RFID tags for calibration-free capacitive/haptic sensor applications," *IEEE Sensors J.*, vol. 15, no. 6, pp. 3135–3145, Jun. 2015.
[34] Y. Xue, B. Hou, S. Wang, Y. Shang, B. Chen, and Y. Ju, "A highly sensitive paper-based chipless RFID humidity sensor based on graphene oxide," *Sens. Actuators A, Phys.*, vol. 358, Aug. 2023, Art. no. 114457.
[35] R. Kruanopparat, "Pressure-measuring devices for compression therapy in venous leg ulcers: A comprehensive review," *Adv. Skin Wound Care*, vol. 34, no. 9, pp. 1–6, Sep. 2021.
[36] B. Kumar, A. Das, and R. Alagirusamy, "An approach to examine dynamic behavior of medical compression bandage," *J. Textile Inst.*, vol. 104, no. 5, pp. 521–529, May 2013.
[37] J. D. Sandt et al., "Stretchable optomechanical fiber sensors for pressure determination in compressive medical textiles," *Adv. Healthcare Mater.*, vol. 7, no. 15, Aug. 2018, Art. no. 1800293.

Minghao Xu received the bachelor's degree from China Jiliang University, Hangzhou, China, in 2020. He is currently pursuing the master's degree with the School of Information and Communication Engineering, Soochow University, Suzhou, China.

His research interests include flexible pressure sensors and wireless communication technology.

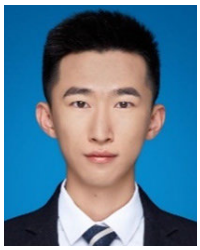

Chenbin Zhao received the bachelor's degree from Soochow University, Suzhou, China, in 2022, where he is currently pursuing the master's degree with the School of Electronic and Information Engineering.

His research focuses on flexible and wearable sensing technology.

Xueguan Liu received the B.S. and M.S. degrees from Xi'an University of Electronic Science and Technology, Xi'an, China, in 1986 and 1989, respectively, and the Ph.D. degree from the Communication University of China/China Aerospace Science and Technology Corporation, Beijing, China, in 2007.

He is currently a Professor and a Ph.D. Supervisor with the School of Electronic Information, Soochow University, Suzhou, China.

Xinjian Chen (Senior Member, IEEE) received the Ph.D. degree from the Institute of Automation, Chinese Academy of Sciences, Beijing, China, in 2006.

After graduation, he joined Microsoft Asia Research Institute, Beijing, as an Associate Researcher. Later, he worked with Ivy League University, the University of Pennsylvania, the National Institutes of Health, and the University of Iowa. In June 2012, he joined Soochow University, Suzhou, China, where he is currently a Distinguished Professor with the School of Electronic and Information Engineering. His research interests cover medical image processing, pattern recognition, image analysis, 3-D modeling, and visualization.

Baoqing Nie received the B.S. degree from Nanjing University, Nanjing, China, in 2010, and the Ph.D. degree from the Department of Biomedical Engineering, University of California at Davis, Davis, CA, USA, in 2015.

She is currently an Associate Professor with the School of Electronic and Information Engineering, Soochow University, Suzhou, China. She has authored or co-authored more than 30 papers in refereed journals and conference proceedings. Her research interests focus on flexible and stretchable sensing devices and biomedical applications.